Journal of Alloys and Compounds 509 (2011) 2099–2104

Contents lists available at ScienceDirect

Journal of Alloys and Compounds

journal homepage: www.elsevier.com/locate/jallcom

Crystal structure and photoluminescence of $(La_{1-x}Ce_x)_5Si_3O_{12}N$

F.C. Lu, X.P. Song, Q.L. Liu*

State Key Laboratory for Advanced Metals and Materials, School of Materials Science & Engineering, University of Science and Technology Beijing, Beijing 100083, PR China

ARTICLE INFO

Article history:
Received 8 September 2010
Received in revised form 13 October 2010
Accepted 27 October 2010
Available online 4 November 2010

Keywords:
$La_5Si_3O_{12}N$
Crystal structure
Ce^{3+} doped
Luminescence

ABSTRACT

Oxonitridosilicate phosphors with compositions of $(La_{1-x}Ce_x)_5Si_3O_{12}N$ ($x = 0$–0.1) have been synthesized. The XRD analyses show that all the compounds are single polycrystalline $La_5Si_3O_{12}N$ phase. La atoms occupy two crystallographic sites in the structure. Two groups of photoluminescence spectra have been observed and can be ascribed to the excitation and emission of the two types of Ce^{3+} photoluminescence centers ($Ce(1)^{3+}$ and $Ce(2)^{3+}$) in the crystallographic sites of La(1) and La(2). The energy transfer between the two types of photoluminescence centers has been discussed. Schematic energy levels of Ce^{3+} ions at the two crystallographic sites are given. Luminescence concentration quenching occurs when Ce content is more than 3 mol%. The quenching temperature is evaluated to be about 406 K for the 3 mol% Ce content sample. This study shows these phosphors potential candidates for application in three-phosphor-converted white LEDs.

1. Introduction

In recent years, solid state lighting has attracted increasing attention by governments and researchers. Compared with incandescent and fluorescent lamps, InGaN-based white light-emitting diodes (WLEDs) show many advantages, such as a long lifetime, a small volume, toxic-free and energy-saving materials [1–3]. There are three different methods that can be used to realize white light emitting: red–green–blue (RGB) light emitting diode (LED) chips combined directly; blue-LED chip combined with yellow (or 'green and red') wavelength conversion phosphor [4,5]; near-ultraviolet LED chip combined with RGB wavelength conversion phosphor [6]. The latter two methods are usually adopted because they are economic and easy for production. In both methods the conversion phosphors are playing an important role. These phosphors must have excellent luminescent features so that they can be efficiently excited by the blue-LED chip or near-ultraviolet LED chip and emit efficiently in blue, green, yellow, or red wavelengths.

Currently large interests have been focused on the Ce^{3+}/Eu^{2+} doped nitridosilicate and oxonitridosilicate due to their potential application as novel phosphors for WLEDs [7]. The emission and absorption spectra of the Ce^{3+}/Eu^{2+} ion usually consist of broad bands due to transitions between the ground state of the $4f^1/4f^7$ configuration and the lower excited states (the crystal field splitting components of the 5d configuration). The emission varies from UV to red, depending on the host lattice because of a strong interaction of the 5d-electron with the neighboring anion ligand in the compounds [8].

The structure of nitridosilicate typically consists of SiN_4 tetrahedra. The nitrogen of SiN_4 tetrahedra can be partially replaced by oxygen to form $Si[O/N]_4$ tetrahedra. SiN_4 or $Si[O/N]_4$ units are stacked together by sharing their corners or edges to form a condensed framework, resulting in excellent thermal and chemical stability of nitridosilicate and oxonitridosilicate. Rare-earth or other metal ions can be accommodated in the voids of the network [9]. These various structures can provide the Ce^{3+}/Eu^{2+} with rich and different ligand environments, and adjust the emission and absorption wavelengths. Some compounds have been extensively studied, such as α-SiAlON [10], β-SiAlON [11], $M_2Si_5N_8:Eu^{2+}$ (M = Ca, Sr, Ba) [12], $Sr_xCa_{1-x}AlSiN_3:Eu^{2+}$ [13] and $Y_4Si_2O_7N_2:Ce^{3+}$ [14]. The above luminescent materials combined the unique luminescence characteristics from 5d to 4f transitions of rare earth ions and thermal and chemical stability of host materials.

In La–Si–O–N quaternary system some crystalline phases have been identified and studied, for example $La_5Si_3O_{12}N$, $La_4Si_2O_7N_2$, $LaSiO_2N$ and $La_3Si_8O_4N_{11}$ [15–17]. But up to now only a few papers have reported the luminescence properties of rare earth doped La–Si–O–N compounds [18]. The reason may be that these compounds always need special synthesis conditions, such as high temperature and high pressure. Moreover, the structures of La–Si–O–N compounds have not been completely identified and studied; while limited interest has been paid to the photoluminescence (PL) properties. In this work, we synthesized a series of Ce doped $(La_{1-x}Ce_x)_5Si_3O_{12}N$ ($x = 0$–0.10) compounds by a novel synthetic route based on a direction reaction among LaSi, CeSi

* Corresponding author at: School of Materials Science & Engineering and State Key Laboratory for Advanced Metals and Materials, University of Science and Technology Beijing, No. 30 Xueyuan Road, Haidian District, Beijing 100083, PR China. Tel.: +86 10 62334705; fax: +86 10 62334705.
E-mail address: qlliu@ustb.edu.cn (Q.L. Liu).

0925-8388/$ – see front matter © 2010 Elsevier B.V. All rights reserved.
doi:10.1016/j.jallcom.2010.10.148

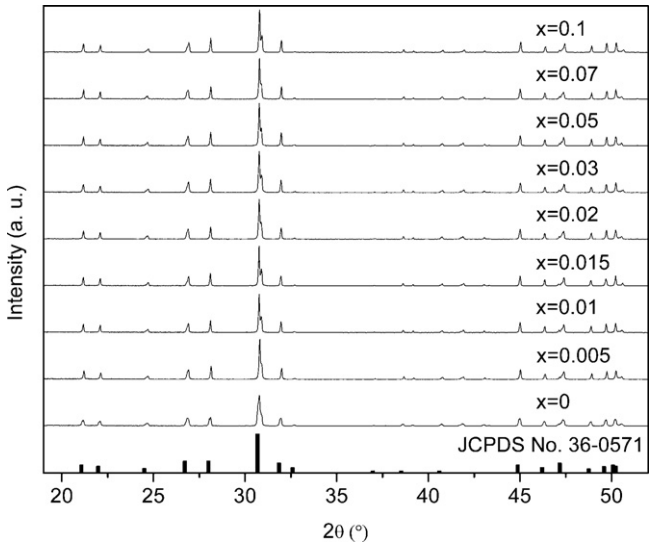

Fig. 1. XRD patterns of $(La_{1-x}Ce_x)_5Si_3O_{12}N$ (x = 0–0.1).

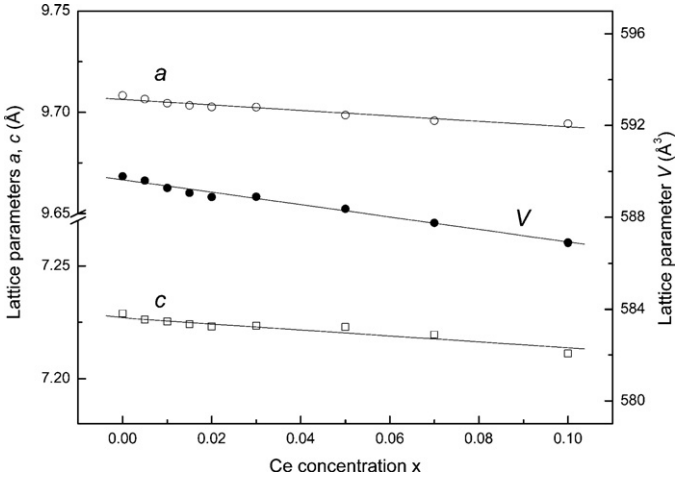

Fig. 2. Variations of parameters a (b), c and V with increasing Ce concentrations.

and La_2O_3 at high temperature and high nitrogen pressure. We investigated their structures and PL properties, and discussed the physical mechanisms for concentration and thermal quenching of these phosphors.

2. Experimental

The starting materials are metallic La, Ce and Si powder and high purity La_2O_3 powder (>99.99%). LaSi and CeSi alloys were firstly prepared by argon arc melting of an appropriate amount of the starting materials. To ensure the homogeneity of the alloys the ingots were turned and melted several times. The raw materials, i.e. LaSi, CeSi, and La_2O_3, were weighed according to the desired compositions, and then mixed, ground and pressed into pellets. Thereafter polycrystalline $(La_{1-x}Ce_x)_5Si_3O_{12}N$ (x = 0, 0.005, 0.01, 0.015, 0.02, 0.03, 0.05, 0.07 and 0.1) samples were prepared by a solid state reaction. The pellets were sintered at about 1823 K for 3 h under high-purity nitrogen atmosphere (>99.999%) in a graphite furnace. The starting nitrogen atmosphere pressure is 0.3 MPa. The samples were cooled down with the furnace. These samples were ground and sintered three times in order to reach equilibrium.

The X-ray diffraction (XRD) data for lattice parameter refinements were collected on a Philips X'Pert PW-3040 diffractometer (45 kV × 40 mA) with Cu $K\alpha_1$ radiation (λ=0.15406 nm). Continuous scan mode with a 2θ scan range of 10–80° was employed. The XRD data for atomic position refinements were collected on a Rigaku D/max 2500 diffractometer (40 kV × 200 mA) with Cu Kα radiation and a graphite monochromator. Step scan mode was employed with a step width of 2θ = 0.02° and a sampling time of 1 s. The 2θ scan range is 10–120°. These XRD data were analyzed by the Rietveld refinement program FullProf.2k (Version 2.40) based on the structure model of $La_5Si_3O_{12}N$ reported by Titeux et al. [15]. A pseudo-Voigt function was used for the profile function.

The PL spectra were measured with an Edinburgh Instruments FLS920 spectrofluorimeter equipped with a continuous (450 W) Xenon lamp. For low and high temperature measurements, the samples were mounted on a closed cycle cryostat (10–450K, DE202, Advanced Research Systems). Slit widths of 0.3 nm each were used on the excitation and emission monochromators. The step width is 1.0 nm and the dwell time is 0.20 s. The line intensities and positions of the measured spectra were calibrated using the FLS920 correction curve and a standard mercury lamp.

3. Results and analyses

3.1. X-ray powder diffractions and structure

The powder XRD patterns of $(La_{1-x}Ce_x)_5Si_3O_{12}N$ (x = 0–0.1) in the region of 20–52° are shown in Fig. 1. The XRD patterns matched well with the reported patterns (JCPDS No. 36-0571) and indicate that these compounds are all single polycrystalline $La_5Si_3O_{12}N$ phase. With increasing Ce concentration, the XRD patterns shift slightly to higher angles. Hence the lattice parameters shrink when more Ce content is added to the material. The results of Rietveld refinements for lattice parameters also show this trend. Fig. 2 shows the relations of the lattice parameters a (b), c and V with Ce concentration. The lattice parameters decrease linearly with increasing Ce concentration, which is in agreement with Vegard's law with a radius of Ce^{3+} (1.03 Å) smaller than that of La^{3+} (1.06 Å). The decreasing linear relation indicates that Ce^{3+} ions have been substituted for La^{3+} ions in the lattice.

As reported by Titeux et al. [15], $La_5Si_3O_{12}N$ belongs to the hexagonal system and the space group is P 6 3/m (No. 176). Its structure has two formula units in a unit cell, i.e. a unit cell contains 10La + 6Si + 24O + 2N atoms. The La, Si, O and N atoms correspondingly occupy 6h + 4f, 6h, 2a + 6h + 6h + 12i and 12i Wyckoff positions in the structure, respectively. The fitted X-ray profile of the Rietveld refinements for $La_5Si_3O_{12}N$ is shown in Fig. 3. In this figure, the middle vertical bars indicate the expected Bragg reflection positions, and the lowest curve is the difference between the observed and calculated patterns. The reliability factors of the Rietveld refinements are Rp = 11.80%, Rwp = 16.10%, Rexp = 11.64%. The equivalent sites and atomic positions are listed in Table 1. The center projection structure of $La_5Si_3O_{12}N$ is shown in Fig. 4(a). The lattice parameters a (b), c and V are 9.7082(1) Å, 7.2279(1) Å and 589.939(3) Å^3, respectively. In the structure La atoms occupy two types of crystallographic sites (Wyckoff positions 6h and 4f). The ratio of the number of La atoms in the two sites is 3:2. La(1) atoms are coor-

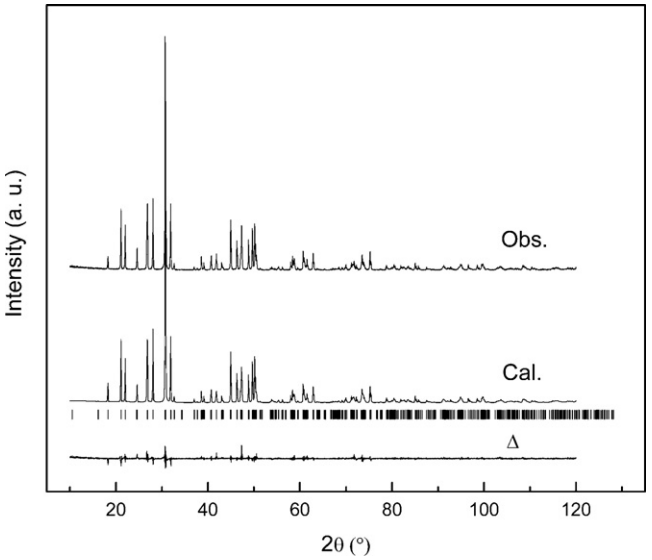

Fig. 3. Observed, calculated and difference XRD patterns of $La_5Si_3O_{12}N$.

Table 1
Atom parameters of $La_5Si_3O_{12}N$.

Atom	Wyckoff position	X	Y	Z	S.O.F.
La(1)	6h	0.2309(3)	−0.0128(3)	0.2500	1.0
La(2)	4f	0.3333	0.6667	0.0006	1.0
Si	6h	0.403(1)	0.378(1)	0.2500	1.0
O(1)	2a	0.0000	0.0000	0.2500	1.0
O(2)	6h	0.316(2)	0.482(2)	0.2500	1.0
O(3)	6h	0.604(2)	0.473(2)	0.2500	1.0
O(4)	12i	0.349(1)	0.256(1)	0.078(2)	0.8333
N	12i	0.349(1)	0.256(1)	0.078(2)	0.1667

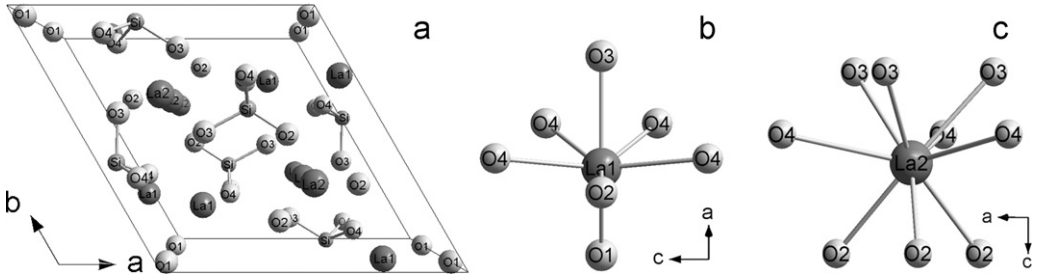

Fig. 4. (a) The center projection structure of $La_5Si_3O_{12}N$. (b) and (c) The coordinated structures of La(1) and La(2) atoms.

dinated by 7 O/N atoms with an average inter-atomic distance of 2.53 Å. La(2) atoms are coordinated by 9 O/N atoms with an average inter-atomic distance of 2.61 Å. The coordinated structures of the two La occupied sites are illustrated in Fig. 4(b).

3.2. Photoluminescence properties

The excitation and emission spectra of the 0.5 mol% Ce content sample are shown in Fig. 5. Two groups of excitation and emission spectra have been observed for this sample. The excitation wavelength (λ_{ex}) is 350 nm and the monitor wavelength (λ_{mon}) is 461 nm for group 1 (spectra 1 and 2 in Fig. 5). For group 2 λ_{ex} is located at 290 nm and λ_{mon} is located at 379 nm (spectra 3 and 4 in Fig. 5). The two groups of PL spectra indicate that there are two types of PL centers in the lattice. As discussed in Section 3.1, La atoms occupy two types of crystallographic sites in the lattice (La(1) and La(2)).When Ce atoms are substituted for La atoms in the lattice, the two types of ligand environments are generating two types of PL centers.

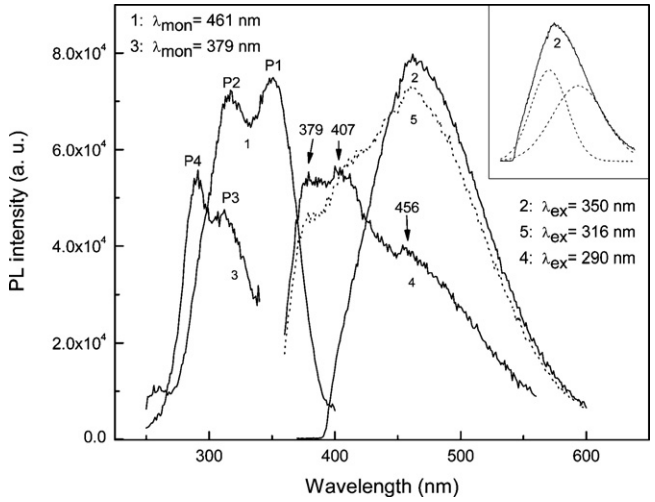

Fig. 5. Emission and excitation spectra of 0.5 mol% Ce content sample.

In the lattice the Ce^{3+} $4f^05d^1$ configuration is intensively disturbed by the crystal field and splits to several energy levels with a maximum of 5. As reported by Dorenbos [19], the intensity of crystal field splitting is inversely proportional to the distance from the coordinate groups to the central cation. As discussed in Section 3.1, La(2) has a larger average inter-atomic distance than La(1). So the 5d energy levels of Ce(1) have a larger crystal field splitting than those of Ce(2). The PL spectra of group 1 belong to the excitation and emission of PL centers of the Ce(1) site and the PL spectra of group 2 belong to those of the Ce(2) site.

The excitation spectrum of group 1 consists of two excitation bands which peak at 350 (P1) and 316 nm (P2). Using λ_{ex} of 350 nm (P1), the emission spectrum shows a structure-less broad band peaking at 461 nm. Using Gaussian functions this emission band can be de-convoluted to two broad bands peaking at 453 nm and 503 nm (shown in the insert figure). The energy gap between the two de-convoluted bands is ~2194 cm^{-1}. As we know, the energy gap between the two spin splitting energies of $^2F_{5/2}$ and $^2F_{7/2}$ for free Ce^{3+} ions is ~2200 cm^{-1} [20]. So the emission of group 1 can be ascribed to the emission of Ce(1) site. Using λ_{ex} of 316 nm (P2), the emission spectrum shows a broad band covering the emissions of groups 1 and 2, as shown with the dotted line in Fig. 5 (spectrum 5).

Using λ_{mon} of 379 nm, the excitation spectrum of group 2 shows two excitation bands peaking at 311 nm (P3) and 290 nm (P4). We think the two excitation peaks (P3 and P4) are generated independently by Ce(2), because the emission intensity of Ce(1) in the wavelength range of less than 400 nm is very weak. So P3 and P4 correspond to the $Ce(2)^{3+}$ transitions from $4f^1$ ground state $^2F_{5/2}$ to the lowest two 5d splitting energies. Using λ_{ex} of 290 nm (P4), the emission spectrum shows a broad band with three emission peaks peaking at 379, 407 and 456 nm. The energy gap between the emission peaks of 379 and 407 nm is ~1815 cm^{-1} and the two emission peaks can be ascribed to the emission of Ce(2). The emission peak of 456 nm can be ascribed to the emission of Ce(1) due to the energy transfer from Ce(2) to Ce(1). Using λ_{ex} of P3, the emission spectrum is similar to that of λ_{ex} at P2.

In the excitation band of group 1, P1 corresponds to $Ce(1)^{3+}$ transitions from the $4f^1$ ground state $^2F_{5/2}$ to the lowest 5d splitting energy. P2 is an overlapping spectrum from the excitation of Ce(1)

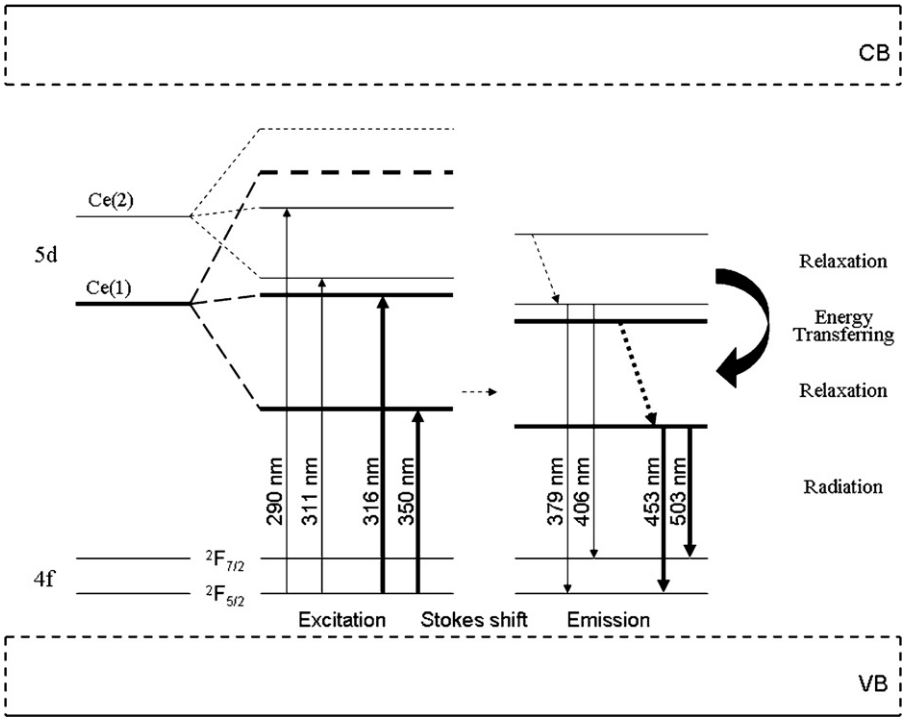

Fig. 6. A systematic energy diagram of Ce^{3+} in the forbidden band of the 0.5 mol% Ce content sample.

and Ce(2). The main proportion is donated by Ce(1) excitation spectrum, corresponding to the transitions of $Ce(1)^{3+}$ $4f^1$ ground state $^2F_{5/2}$ to the second lowest 5d splitting energy. The remaining proportion is donated by the Ce(2) excitation spectrum, corresponding to the transitions of $Ce(2)^{3+}$ $4f^1$ ground state $^2F_{5/2}$ to the lowest 5d splitting energy (same to P3 of group 2). This is because under λ_{ex} of P2 the emission spectrum (spectrum 5 in Fig. 5) covers the two groups of emissions of Ce(1) and Ce(2). And because the emission spectra of λ_{ex} at P2 and P3 are nearly the same, we think the second lowest 5d splitting energy of Ce(1) is close to the lowest 5d splitting energy of Ce(2).

Based on the analyses mentioned above, a schematic energy diagram of $Ce(1)^{3+}$ and $Ce(2)^{3+}$ in the forbidden band of the 0.5 mol% Ce content sample is given in Fig. 6.

With increasing Ce content in the material the PL intensity of group 2 decreases. For the Ce content $x > 0.05$ samples only the PL spectra of group 1 are observed. That is because the increasing Ce content in the lattice leads to an efficient energy transfer from Ce(2) to Ce(1) site (as illustrated in Fig. 6) and only the emission of Ce(1) is occurring for higher Ce content samples. With increasing Ce concentrations from 0.5 mol% to 10 mol%, the emission peak (group 1) red-shifts from 461 to 470 nm (shown in Fig. 7(a)). The excitation peak of P1 also shows red shifts from 350 to 359 nm with the increasing Ce concentrations (shown in Fig. 7(b)). For comparison, in Fig. 8 the PL spectra of group 1 in 0.5 mol%, 3 mol% and 10 mol% Ce samples are drawn together. With increasing Ce content in the lattice, the crystal splitting is increasing and lowers the 5d splitting energies. Then the excitation and emission peaks shift to longer wavelengths. Contrary to P1, the excitation peak P2 shows blue shifts from 316 to 312 nm for Ce concentrations of 0.5 mol%–10 mol% (shown in Fig. 7(c)). The reason may be that with increasing Ce concentration, in the excitation band of P2 the excitation energy donated by Ce(2) is becoming stronger (although the emission of Ce(2) decreased because of energy transfer), and then this excitation peak shifts to shorter wavelengths towards the excitation peak of P3.

From Fig. 8 we can see with increasing Ce content the PL intensity ratio of P1 to P2 increases. The ratio varied from ~1:1 to ~3:2. For the lower Ce content samples the Ce atoms preferably occupy the La(2) site because La(2) has a larger polyhedron than that of La(1). Hence the intensity ratio of P1 to P2 is lower. With increasing Ce content in the lattice, the Ce atoms tend to be distributed equally over the La(1) and La(2) sites. The intensity ratio of P1 to P2 becomes higher. For the 10 mol% Ce content sample, the value approaches the ratio of the number of La(1) to La(2) atoms in the lattice.

With increasing Ce content, concentration quenching occurs. Concentration quenching usually occurs as a result of non-radiative energy transfer among luminescence centers. Two mechanisms are usually adopted to explain the non-radiative energy transfer, i.e.,

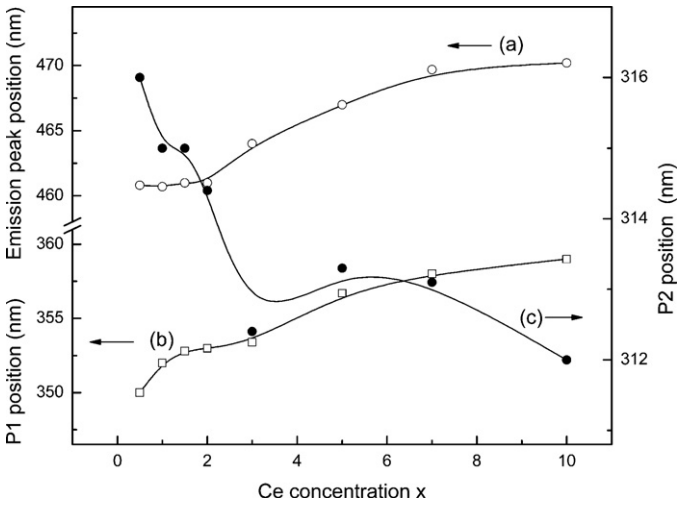

Fig. 7. Variations of the positions of excitation and emission peaks with increasing Ce concentrations.

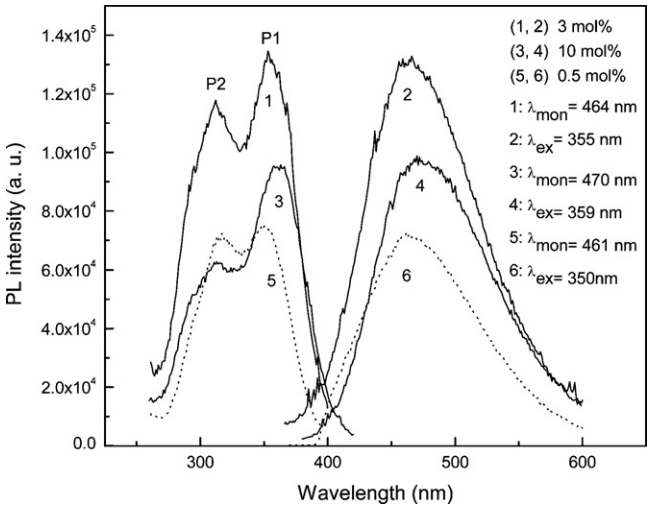

Fig. 8. PL spectra of 0.5 mol%, 3 mol% and 10 mol% Ce content samples.

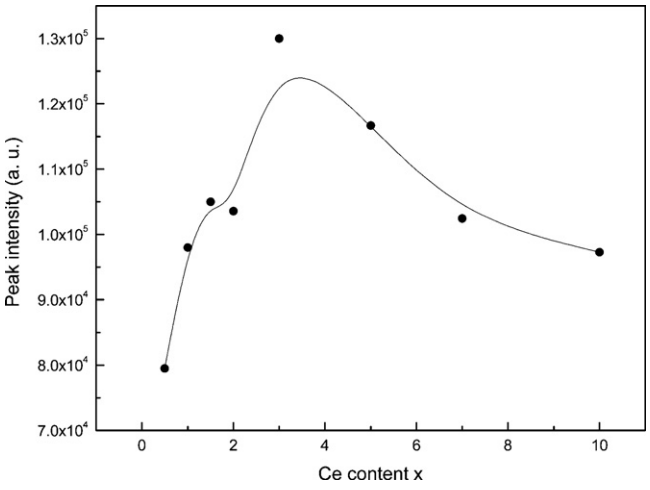

Fig. 9. Variation of the PL intensity with increasing Ce concentrations.

multipolar interaction and radiation re-absorption. In the mechanism of multipolar interaction, the probability of energy transfer between two activator ions is inversely proportional to the nth power of R' (n = 6, 8, or 10) where R' is the distance between the activator ions [18,21]. With increasing Ce content in the lattice, the inter-atomic distance between the two activators becomes smaller, and then the probability of energy transfer becomes higher. On one hand the energy transfer between the activators quenches the PL intensities. On the other hand Ce(2) transfers the excitation energy to Ce(1), leading to the disappearance of the PL spectra of group 2 for the higher Ce content samples.

Because there is some overlap between the excitations and emissions (see Fig. 8), the mechanism of radiation re-absorption may also be playing an important role for the concentration quenching in this material. In addition, with increasing Ce concentration the re-absorption reduced the high-energy wing of the Ce^{3+} emission band and red shifted the emission peaks. In this material the concentration-dependent PL intensities are illustrated in Fig. 9. The best doping Ce content is 3 mol%, a relative low concentration.

The PL spectra of the 3 mol% Ce content sample in the temperature range of 10–350 K have been measured. Fig. 10 shows the results at temperatures of 10, 150, 250 and 350 K. As shown in the figure, the excitation and emission intensities decrease with increasing temperature, i.e. thermal quenching. Several mechanisms can be used to explain thermal quenching of phosphors. A widely accepted mechanism is the electronic transition through the intersection between the ground and excited states, in other words this mechanism is described as a large displacement between the ground and excited state in the configuration coordinate diagram [22]. Other quenching mechanisms, for example thermal excitation of 5d electrons to conduction band sates [23] or excitation of holes from Ce to the valence band states [24], were also suggested [25]. With increasing temperature the PL intensities of each excitation and emission decrease because of thermal quenching. Note that, as shown in Fig. 10, the intensity of P2 decreases more quickly than that of P1. At 10 K, P2 has a higher intensity than P1. At 350 K, the

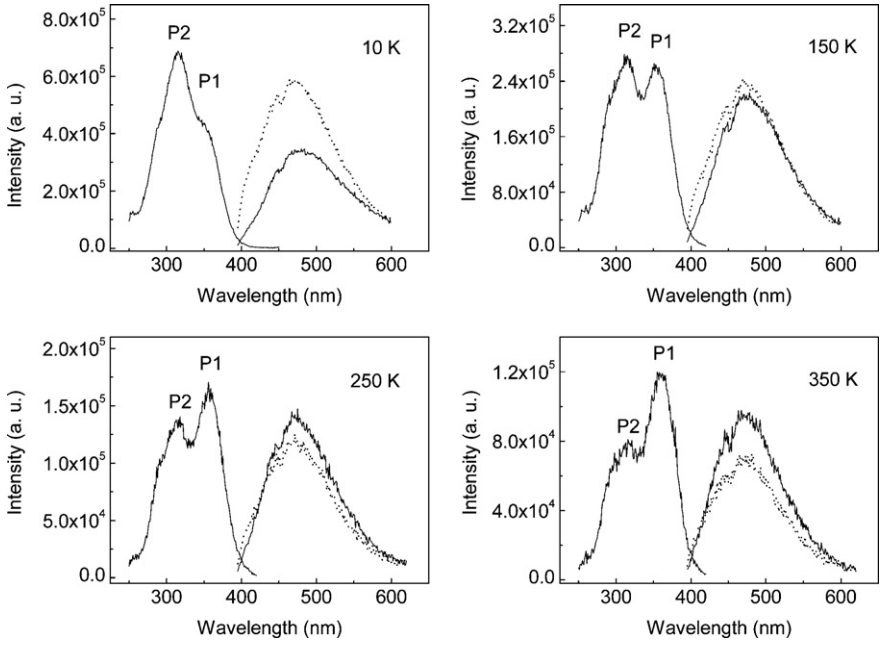

Fig. 10. Excitation and emission spectra of 3 mol% Ce content sample measured at 10, 150, 200 and 350 K. For the emission spectra, the solid-line showed the emissions of λ_{ex} at P1, the dot-line showed that of λ_{ex} at P2.

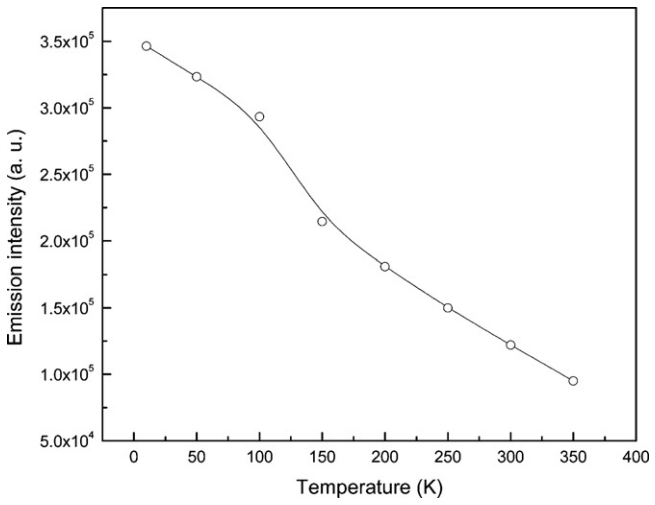

Fig. 11. Temperature-dependent emission intensities of the 3 mol% Ce content sample.

intensity of P1 is higher than that of P2. This phenomenon can be explained with the mechanism of thermal excitation of 5d electrons to conduction band sates. Reference to the energy diagram showed in Fig. 6, the 5d energy levels of Ce(2) are higher than those of Ce(1). The energy gap between the lowest 5d energy level and the conduction band (CB) of Ce(2) is smaller than that of Ce(1). Under thermal excitation the 5d electrons of Ce(2) are easier to be excited to the CB than those of Ce(1). So with increasing temperature the intensity of P2 decreases more quickly than that of P1.

From the temperature of 10–350 K the excitation and emission bands nearly showed no shift. That is the Stokes shift of this phosphor was stable against temperature. This may be because this material has a rigid structure framework of $Si[O/N]_4$ tetrahedra. Hence the chromaticity coordinates of the excitation and emission spectra of this phosphor are stable with temperature. When the temperature is higher than 200 K, the emission intensity of λ_{ex} at P1 is becoming stronger than that of λ_{ex} at P2. In this part, our discussion emphasis is focused on the emission spectrum of group 1 (i.e. λ_{ex} at P1). Fig. 11 shows the temperature-dependent emission intensities of λ_{ex} at P1 in the temperature range of 10–350 K. The data were fitted with a Boltzmann model. For this phosphor, the quenching temperature, defined as the temperature at which the emission intensity drops 50% of that measured at 300 K, can be estimated as 406 K.

4. Conclusions

We have synthesized oxonitridosilicate phosphors with composition $(La_{1-x}Ce_x)_5Si_3O_{12}N$ (x = 0–0.1) by solid-state reaction, and reported the effects of the activator Ce^{3+} concentration on the crystal structure and luminescent properties. The analyses of the XRD patterns show that all the compounds are single polycrystalline $La_5Si_3O_{12}N$ phase. The lattice parameter refinements show that with increasing Ce concentration the lattice parameters a (b), c, and V decrease linearly, i.e. Ce^{3+} has been substituted for La^{3+} in the lattice. Two groups of PL spectra have been observed and can be ascribed to the excitation and emission of the two types of PL centers in the lattice, in agreement with the crystal structure in which La atoms occupied two crystallographic sites. When Ce atoms are substituted for La atoms, the different ligand environments generate two types of PL centers. With increasing Ce concentration the PL spectra of group 2 decrease because of energy transfer. With Ce content more than 5 mol%, the PL spectra of group 2 disappeared. The optimum Ce content for the $(La_{1-x}Ce_x)_5Si_3O_{12}N$ phosphors is 3 mol%. The PL properties of the 3 mol% Ce content sample at the different temperatures showed that the chromaticity coordinates of the excitation and emission spectra of this phosphor are stable against temperature. For these phosphors the excitation spectra covered a broad band of 300–400 nm and the emission of 450–550 nm. These phosphors can efficiently convert near-ultraviolet to blue light, providing potential candidates for applications in three-phosphor-converted WLEDs.

Acknowledgements

This work is supported by National Natural Science Foundation of China (No. 90922027) and the National High Technology Research and Development Program of China (No. 2009AA03Z432).

References

[1] S. Nakamura, T. Mukai, M. Senoh, Appl. Phys. Lett. 64 (1994) 1687.
[2] X.D. Wei, L.Y. Cai, F.C. Lu, X.L. Chen, X.Y. Chen, Q.L. Liu, Chin. Phys. B 18 (2009) 3555–3562.
[3] L.Y. Cai, X.D. Wei, H. Li, Q.L. Liu, J. Lumin. 129 (2009) 165–168.
[4] P. Schlotter, J. Baur, Ch. Hielscher, M. Kunzer, H. Obloh, R. Schmidt, J. Schneider, Mater. Sci. Eng. B 59 (1999) 390–394.
[5] R. Mueller-Mach, G.O. Mueller, M.R. Krames, T. Trottier, IEEE J. Sel. Top. Quant. Elect. 8 (2002) 339.
[6] K. Kobashi, T. Taguchi, Proc. SPIE 5739 (2005) 25.
[7] R.-J. Xie, N. Hirosaki, K. Sakuma, Y. Yamamoto, M. Mitomo, Appl. Phys. Lett. 84 (2004) 5404.
[8] N. Hirosaki, R.-J. Xie, K. Kimoto, T. Sekiguchi, Y. Yamamoto, T. Suehiro, M. Mitomo, Appl. Phys. Lett. 86 (2004) 211905.
[9] Y.Q. Li, J.E.J. van Steen, J.W.H. van Krevel, G. Botty, A.C.A. Delsing, F.J. DiSalvo, G. de With, H.T. Hintzen, J. Alloys Compd. 417 (2006) 273.
[10] H. Watanabe, N. Kijima, J. Alloys Compd. 475 (2009) 434.
[11] P. Dorenbos, J. Lumin. 91 (2000) 155.
[12] P. Dorenbos, J. Lumin. 104 (2003) 239.
[13] R. Niewa, F.J. DiSalvo, Chem. Mater. 10 (1998) 2733.
[14] F.C. Lu, X.P. Song, Q.L. Liu, Opt. Mater. 33 (2010) 91.
[15] S. Titeux, M. Gervais, P. Verdier, Y. Laurent, Mater. Sci. Forum 17 (2000) 325–326.
[16] J. Takahashi, H. Yamane, N. Hirosaki, Y. Yamamoto, T. Suehiro, T. Kamiyama, M. Shimada, Chem. Mater. 15 (2003) 1099–1104.
[17] R.K. Harris, M.J. Leach, Chem. Mater. 4 (1992) 260–267.
[18] B. Dierre, R.-J. Xie, N. Hirosaki, T. Sekiguchi, J. Mater. Res. 22 (2007) 1933–1941.
[19] P. Dorenbos, J. Alloys Compd. 341 (2002) 156.
[20] R.R. Jacobs, W.F. Krupke, M.J. Weber, Appl. Phys. Lett. 33 (1978) 410–412.
[21] J. Qiu, K. Miura, N. Sugimoto, K. Hirao, J. Non-Cryst. Solids 266 (1997) 213–214.
[22] G.H. Munoz, C.L. de la Cruz., A.F. Munoz, J.O. Rubio, J. Mater. Sci. Lett. 7 (1988) 1310–1312.
[23] U. Happek, S.A. basun, J. Choi, J.K. Krebs, M. Raukas, J. Alloys Compd. 198 (2000) 303–304.
[24] H. Najafov, A. Kato, H. Toyota, K. Iwai, A. Bayramov, S. Iida, Jpn. J. Appl. Phys. 41 (2002) 2058–2065.
[25] P. Dorenbos, J. Phys.: Condens. Mater. 17 (2005) 8103–8111.